Journal of Materials Chemistry C

Accepted Manuscript

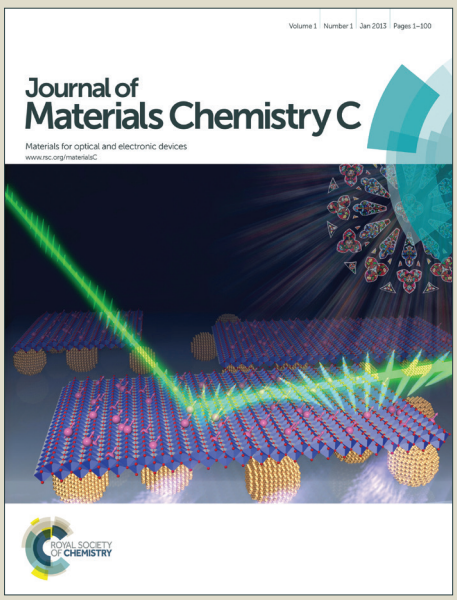

ROYAL SOCIETY OF CHEMISTRY

www.rsc.org/materialsC

Journal of Materials Chemistry C RSCPublishing

COMMUNICATION

Independent Chemical/Physical Role of Combustive Exothermic Heat in Solution-Processed Metal Oxide Semiconductors for Thin-Film Transistors

Cite this: DOI: 10.1039/xoxxoooooox

Received ooth January 2012,
Accepted ooth January 2012

DOI: 10.1039/xoxxoooooox

www.rsc.org/

Seong Jip Kim,[a] Ae Ran Song,[b] Sun Sook Lee,[a] Sahn Nahm,[c] Youngmin Choi,[a,*] Kwun-Bum Chung,[d,*] Sunho Jeong[a,*]

Abstract
The development of high performance, solution-processed metal-oxide semiconductors have been of paramount interest in various fields of electronic applications. Among the variety of methodologies for synthesizing solution-processed precursor solutions, the combustion chemistry reaction, which involves an internal exothermic heat reaction, has drawn tremendous attraction as one of the most viable chemical approaches. In this paper, we report the synthesis of new zinc-tin oxide (ZTO) precursor solutions that can be used to independently adjust the amount of combustive exothermic heat. Through comparative analyses based on X-ray photoelectron spectroscopy, spectroscopic ellipsometry, and X-ray absorption spectroscopy, the independent influence of combustive heat is elucidated in indium-free, solution-processed oxide semiconductors, in conjunction with an interpretation of observed variations in device performance.

In the past decade, solution-processed metal oxide semiconductors (MOSs) have attracted tremendous attention in the field of optoelectronic devices, owing to their device performance, which is superior to amorphous Si and organic semiconductors, as well as their low cost and scalable deposition processability.[1,2] When combined with next-generation deposition techniques such as the direct-writable printing method, high-performance solution-processed MOSs can be patterned arbitrarily on demand, and have been successfully implemented in device architectures of thin-film transistors.[3,4] In the early stages of solution-processed MOS applications, thermal annealing at high temperature was required to generate device-quality channel layers for thin-film transistors (TFTs). This required heat levels at which even glass substrates do not stably survive. Recently, by virtue of newly developed chemical approaches and post-treatment methodologies, potential alternatives to vacuum deposited counterparts have been suggested, with demonstrated mobilities exceeding 10 $cm^2/V \cdot s$.[5-11] Among them, deep UV (which accompanies photo-chemical triggering of metal oxide-framework formation reactions[12]), and combustion chemistry-involved pathways,[13-17] have been recognized as viable approaches for low temperature-annealed, high-performance solution-processed MOSs. In particular, the use of noble chemical pathways could be a more meaningful strategy, since these allow for various combinatorial approaches, when combined with proper post-treatment processes, depending on the chemical/physical states of the synthesized precursors.

The combustion chemistry needs a pair-reaction initiated by a fuel and an oxidizer. The internal heat generated by an exothermic combustive explosion in thin oxide films enables the efficient chemical conversion of precursors into metal oxide skeletons at low temperatures. To date, two representative ways of driving the fuel-oxidizer pair reactions have been suggested: i) using a metal nitrate precursor as a fuel, and acetylacetone or urea as an additionally incorporated oxidizer;[13] or ii) using a metal nitrate precursor as a fuel and a metal acetylacetonate precursor as an oxidizer.[17] According to semi-statistical analysis in a previous study, the latter approach, which is called a self-combustion reaction because the chemical contribution of fuel and oxidizer is derived only in the form of precursors, has proven more reproducible owing to the simplicity of the synthesis reactions. However, the influence of combustion chemistry was not independently investigated because the cation composition, a critical factor determining device performance of MOS-TFTs, is linked with the ratio of fuel to oxidizer and cannot be varied separately. This give rises to some ambiguity regarding the role of the exothermic combustion reaction, in both the chemical structural evolution in oxide films and in device performance. Moreover, to date, analytical information on the evolution of the physical/electronic structures of these oxide systems has not been established, and indium has been predominantly incorporated as a mobility enhancer for improving device performance, despite of the economic issues as an earth-rare element.

Herein, we report on our investigation of the independent role of combustive exothermic heat in evolving the chemical/physical structure of indium-free, Zn-Sn-O (ZTO) MOS-TFTs, by adjusting the combustion-pair reaction in metal oxides, with an equivalent elemental ratio of Zn to Sn. For this study, we design new ZTO precursor solutions for combustion chemistry. Based upon comparative spectroscopic analyses using X-ray photoelectron spectroscopy (XPS), spectroscopic

ellipsometry (SE), and X-ray absorption spectroscopy (XAS), the origins of significant improvement in device performance is elucidated for the combustion reaction-involved, solution-processed metal-oxide semiconductors.

The ZTO precursor solutions were prepared using ammonium nitrate and metal salts of zinc acetylacetonate and tin chloride. After film forming and drying, fuel-oxidizer pair chemical moieties should be established in the solvent-free films, in order to trigger the combustion reaction during conventional thermal annealing. The difficulty in preparing combustion chemistry-derived ZTO-precursor solutions is associated with the absence of commercially available tin acetylacetonate, and with the extreme instability of tin nitrate in ambient air. An alternative approach, a chemical methodology for synthesizing the nitrate salt of tin in an alcohol medium, has been reported. It involves the reaction between tin chloride and ammonium nitrate,[13] in which the volatile ammonia is vaporized at low temperatures, as proven in the synthetic scheme of producing Zn hydroxide.[18] In our precursor systems, the amount of combustive exothermic heat can be determined by the composition of incorporated ammonium nitrate in relation to the Zn acetylacetonate, while maintaining a constant Zn/Sn ratio.

Firstly, in order to monitor the thermal behavior of each ZTO precursor, the differential thermal analysis (DTA) was carried out for ZTO precursors having different ratios of ammonium nitrate to Zn acetylacetonate (Figure 1). The molar ratio of ammonium nitrate to Zn acetylacetonate is denoted as R, and ZTO precursors with R-values of 0, 1, and 2 are described as R0-, R1-, and R2-ZTO, respectively. Under synthetic conditions with R-values over 3, significant precipitates were formed during the process of synthesizing the precursor solutions. The ZTO precursors used for DTA measurements were prepared by drying the excessive solvents at 80 °C under vacuum. In the as-synthesized precursor solutions, predominant endothermic peaks produced by solvent evaporation shadowed the endo/exothermic peaks from other reactions. The R0-ZTO precursors, which do not undergo a combustion reaction, could not be obtained in a semi-solid phase, even after drying for a prolonged time. This indicates that a slight solidification reaction resulting from partial combustive sol-gel reactions might occur to some extent in R1- and R2-ZTO precursors during drying at 80 °C. Even with these slightly pre-reacted chemical states, a different thermal behavior was distinctly observed for the quantitatively varied fuel-oxidizer pair reactions. Whereas a small exothermic peak was detected around 103 °C for R1-ZTOs, the R2-ZTOs exhibited huge exothermic peaks at 87 °C. According to the Figure S1, the thermal decomposition of impurities were complete around 100 °C, which is almost corresponding to the triggering temperature of combustive exothermal heat in both ZTO films. This indicates that the combustive heat play a critical role in leading to the complete decomposition of impurities. However, in soluble precursors for oxides, the additional supply of thermal energy should be involved for deriving further the stepwise sol-gel reactions and the physical/chemical structural relaxations; those subsequent reactions are associated with other peaks/troughs above 200 °C. An apparent endothermic reaction evolved at 335 °C for R1-ZTOs, but was not observed with R2-ZTOs. This implies that there was insufficient internal heat for R1-ZTOs, caused by a sub-optimum oxidizer/fuel pairing ratio, and that further reactions proceeded by absorbing externally supplied heat. In contrast, for the R2-ZTOs, almost enough exothermic thermal energy was generated inside the precursor

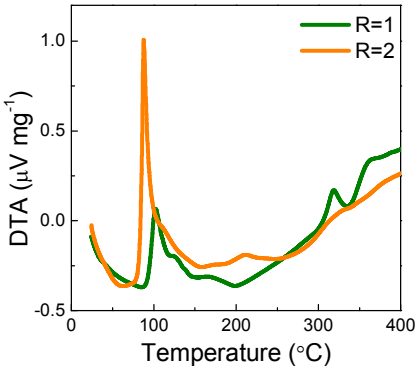

Figure 1. Thermal behavior of ZTO semiconductors derived from precursor solutions with R values of 1 and 2. The molar ratio of Zn to Sn was 1, and the heating rate was 5 °C/min.

films to complete the main reaction below 100 °C; then, subtle additional reactions and temperature-dependent relaxation of the physical structure occurred at higher temperatures.

Figure 2 shows the transfer characteristics and the variation of device performance parameters, including field-effect mobility and threshold voltage, for ZTO-TFTs with R-values from 0 to 2. The saturation mobilities were extracted from the forward-sweep curves of transfer characteristics. All of devices tested in this study were fabricated by depositing the precursor solutions on 100 nm-thick SiO_2/n^+-Si substrates, followed by thermal annealing at 350 °C. Aluminum was then thermally evaporated through shadow masks with a channel length of 100 um and a width of 1000 um. As shown in Figure 2a, mobility was improved by a factor of 11 (from 0.3 to 3.3 $cm^2/V{\cdot}s$) by increasing the R-values from 0 to 1. As seen in Figure S2, the mobility for TFT employing the R0-ZTO channel layer can be underestimated due to insufficient charge accumulation caused by a high threshold voltage. However, in amorphous oxide semiconductors, channel layers with high threshold voltages tend to suffer from low concentration of charge-carriers, which in turn limits field-effect mobility, even when a sufficient gate voltage is applied.[3,4] Thus, it was presumed that the mobility of R0-ZTO TFTs would be much less than those of R1- and R2-ZTO TFTs, owing to the intrinsic chemical/electrical properties, discussed later in this study. This variation of field-effect mobility in ZTO devices, demonstrates the distinct effectiveness of the combustion reaction in generating high-performance, solution-processed metal-oxide TFTs, without the need for ambiguous interpretation of the variation of the metal-cation compositional ratio. The field-effect mobility was further enhanced (to 7.8 $cm^2/V{\cdot}s$) in R2-ZTO-based TFTs by providing more internal exothermic heat. To date, the field-effect mobility of solution-processed ZTO-based TFTs has achieved values even above 10 $cm^2/V{\cdot}s$,[19] but mobilities for annealing temperatures below 400 °C have been limited to around 3 $cm^2/V{\cdot}s$.[20] Effective combustion chemistry has not been implemented in ZTO material systems, and In-added materials such as In_2O_3, In-Zn-O, and In-Ga-Zn-O have been derived by combustion reactions, showing mobilities of around 7-8 $cm^2/V{\cdot}s$.[13,17] The acceptable annealing temperatures for practical applications are below 400 °C, at which the rigid glass substrate can stably survive; the issues for low-temperature annealing compatible to thermally vulnerable plastic substrates have not prevailed practically due to the current technological status in depositing other layers including gate insulators and

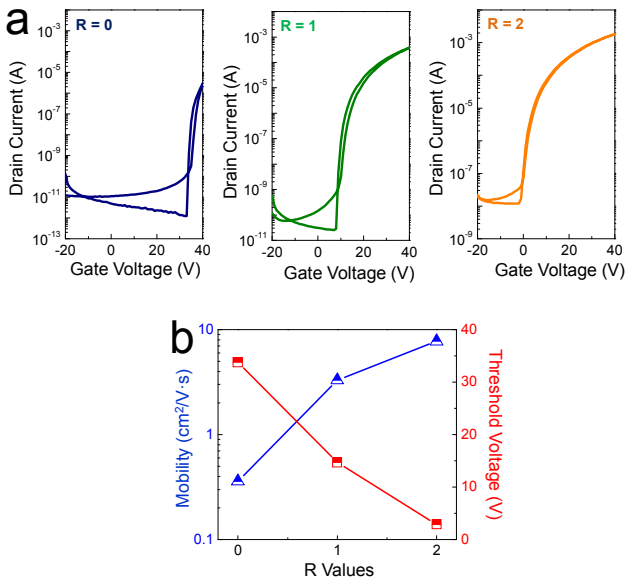

Figure 2. (a) Transfer characteristics and (b) variation of device performance parameters, field-effect mobility and threshold voltage, for TFTs employing ZTO channel layers from precursor solutions with R values of 0, 1, and 2. The molar ratio of Zn to Sn was 1. In transfer characteristics, the drain voltage of 40 V was applied for all devices.

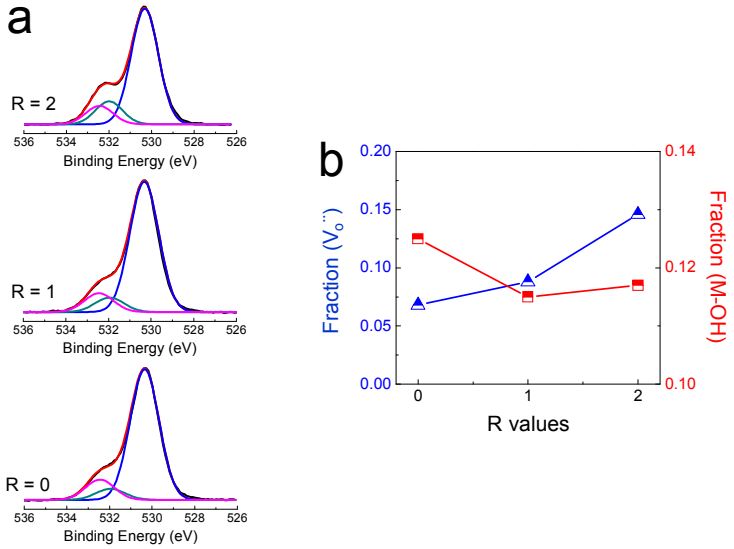

Figure 3. (a) XPS O 1s spectra and (b) semi-quantitative analysis results for ZTO channel layers from precursor solutions with R values of 0, 1, and 2. The molar ratio of Zn to Sn was 1.

passivation films. Considering only field-effect mobility, this mobility approaching 8 $cm^2/V{\cdot}s$ is close to that of vacuum-deposited metal-oxide semiconductors that are industrially commercialized.[21] In R2-ZTO TFTs, when the annealing temperature decreased further down to 300 ^oC, the mobility of 1.2 $cm^2/V{\cdot}s$ was obtained, and at the annealing condition below 250 ^oC, the mobility was drastically degraded (Figure S3).

The change in threshold voltage as a function of the R-value was also in accordance with the trend in field-effect mobility. The threshold voltage shifted significantly, from 33.8 to 2.9 V, closer to 0 V, with increasing R-values. The high threshold voltage is tentatively associated with defect states, where charge carriers are trapped; thus, the threshold voltage would shift positively for n-type solution-processed oxide transistors employing channel layers annealed with insufficient thermal energy.[22,23] The variation of threshold voltage in forward/backward sweeps also decreased depending on R-values, showing hysteresis behavior of 4.1, 3, and 1.7 V for R0, R1, and R2-ZTO TFTs, respectively. This distinctively different device performance was not associated with morphological and crystalline structural properties. As shown in Figure S4-6, regardless of R-values, no noticeable difference was observed in high-resolution transmission-electron-microscopy images, atomic-force-microscopy images, and X-ray diffraction results; they all indicate films with identically densely-uniform, smooth, amorphous properties.

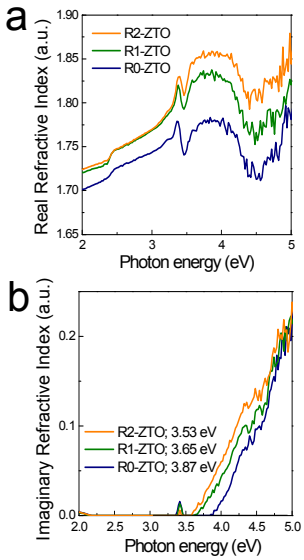

Figure 4. (a) Real part of complex refractive index (n), and (b) imaginary part of complex refractive index (k), measured by SE, for R0, R1, and R2-ZTO channel layers. The numbers next to sample indices in (b) indicate the optical bandgap for each ZTO layer.

To obtain in-depth information on the evolution of chemical, physical, and electronic structures according to the degree of combustive reactions, we carried out spectroscopic analyses based on X-ray photoelectron spectroscopy (XPS), spectroscopic ellipsometry (SE), and X-ray absorption spectroscopy (XAS). Figure 3a shows the XPS O 1s spectra for R0-, R1-, and R2-ZTO channel layers. Prior to the interpretation on O 1s spectra, we calculated the compositional ratio of Zn to Sn for all of ZTO films based on the areal integration for Zn 2p and Sn 3d peaks. The atomic ratios of Zn/Sn were measured to be 1.03, 1.02, and 1.01 for R0-, R1-, and R2-ZTO films, respectively. The peaks, positioned at 530.4 and 532 eV, are due to the oxide lattice without oxygen vacancies, and with oxygen vacancies, respectively.[24,25] The peak at 532.5 eV is attributed to the hydroxyl group.[9,26] In previous studies of diverse cases of solution-processed metal oxides, it was suggested that metal oxide frameworks composed of less hydroxides and more oxygen vacancies should be evolved in order to obtain high performance devices.[3,4,13,27,28] Because the presence of hydroxide tends to create defect trap sites for electrons and the oxygen vacancy formation contributes to the generation of charge carriers,[29] field-effect mobilities are improved dependently along with the negative shift of threshold voltage. According to the semi-quantitative analytical results obtained by the individual areal integration of sub-peaks (Figure 3b), the fraction of oxide lattices with oxygen vacancies was gradually increased as a function of R-values, and the fraction of hydroxide abruptly decreased at an R-value of 1. That level was approximated for R-values of 1-2. It is speculated that this chemical structural evolution is closely related to the abrupt improvement in device performance of R1-ZTOs. The effect might be produced by combinatorial activation in both of the oxide framework-formation reaction, consuming hydroxides, and the generation of oxygen vacancies. The gradual enhancement in R2-ZTOs is attributable solely to the further evolution of oxide lattices with oxygen vacancies.

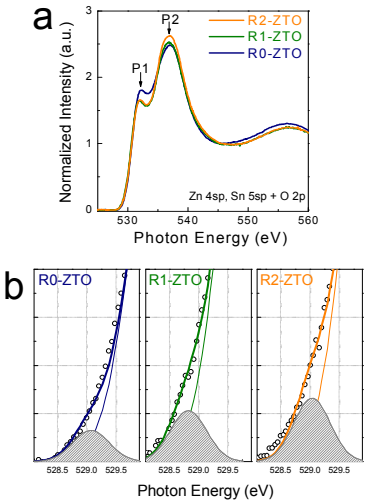

Figure 5. (a) O-K edge XAS spectra and (b) enlargement of band-edge states below the conduction band edge for R0, R1, and R2-ZTO channel layers.

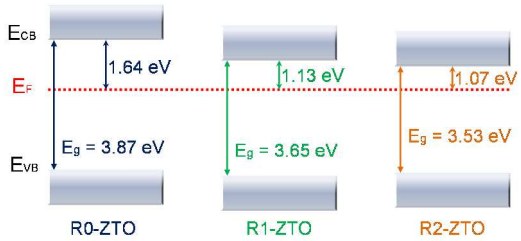

Figure 6. Schematic energy diagram, reflecting the relative energy position of the Fermi level (E_F) with respect to the conduction-band minimum and valence-band maximum, for R0, R1, and R2-ZTO channel layers.

To understand the optical properties, complex refractive index (ñ = n + ik), and SE spectra were measured for all of the ZTO layers. These spectra were extracted from a simple four-phase model, comprised of a substrate, interface, ZTO over-layer, and an ambient layer.[30] As shown in Figure 4a, the real part of the complex refractive index, which is related to film density, increased as a function of the R-value. The imaginary part of the complex refractive index reflects the absorption property of the ZTO film itself. The optical band gap (E_g) was extrapolated from it, and was comparable with previous results (3.3–3.7 eV).[31,32] It was revealed that the optical bandgap of ZTO films decreased by 0.34 eV as the R-value increased from 0 to 2 (Figure 4b). It is believed that the optical bandgap is varied by the changes of oxygen coordination due to the presence of oxygen vacancies and the different metal-oxygen bonding nature. A dense inorganic semiconducting layer with narrower optical bandgap, is capable of reducing defects in the interfacial channel layer adjacent to a dielectric, and in turn, capable of enhancing charge-carrier transport from occupied states to the conduction band. It is believed that this contributed to the improvement of device performance in ZTO layers experiencing more combustive heat.

Figure 5a shows the normalized O-K edge XAS spectra, which provides more information over a wider conduction band, as well as the unoccupied hybridized states between Zn 4sp, Sn 5sp, and O 2p produced by the transition of electrons from

occupied O 1s.[33] The normalization of the O-K edge-spectra was performed by subtracting the X-ray background and scaling the post-edge levels to a uniform value.[34] The feature of the conduction band appeared to be modified slightly as a function of the R-value. As the R-value increased from 0 to 2, the P1 peak at a lower photon energy decreased, and the P2 peak at a higher photon energy increased. This spectral evolution implies that sp-orbital hybridization, rather than that of the s-orbital, strengthened and was induced by changes in the orbital ordering of ZnO and SnO caused by exothermic combustive heat. Another interesting finding involves variation in the conduction-band edge (Figure 5b). In order to examine the conduction-band edge in more detail, Gaussian fits were performed. Previous studies of metal oxides indicated the correlation between band-edge states and electrical properties such as carrier concentration and mobility.[35-37] According to results from previous investigations, the increase of shallow band-edge states is associated with changes of electronic structure, and is mainly attributable to increase in charge-carrier concentration.[38] The increase in charge-carrier concentration in the band-edge state, depending on R-value, can be interpreted as an increase of oxygen vacancies. This corresponds well with the aforementioned XPS results.

Figure 6 shows a schematic energy diagram based on the value of bandgap (E_g) from SE data, and the valence band offset (ΔE_{VB}) from the Fermi level (E_F) obtained using the extrapolation method in the valence band XPS spectra (Figure S7). It was clearly observed that the relative energy difference between E_F and the conduction band minimum (ΔE_{CB}), was reduced by 0.44 eV as the R-value increased from 0 to 2. This result is strongly correlated to the increase in carrier concentration, which is another plausible basis for enhancement of device performance.

In summary, we have designed high performance, solution-processed ZTO precursors with independently controllable levels of combustive exothermic heat, by incorporating zinc acetylacetonate, tin chloride, and ammonium nitrate in an alcohol medium. It was revealed that the exothermic heat was adjustable as a function of the R-value representing the molar ratio of ammonium nitrate to zinc acetylacetonate, while the ratio of Zn to Sn was maintained at 1. XPS, SE, and XAS-based spectroscopy analyses clearly demonstrated that combustive heat plays a critical role in evolving a chemical structure with more oxygen vacancies and less hydroxides. In addition, physical/electronic structures with a higher film density, a lower bandgap, a narrower gap between ΔE_{CB} and E_F, and enhanced shallow band-edge states were evolved when more exothermic heat was involved, resulting in improved device performance. It is believed that the spectroscopic investigation in this study elucidates plausible origins of the correlation between device performance and evolution of chemical/physical structure in combustion chemistry-involved oxide semiconductors.

Acknowledgements

This research has been supported by the Korea Research Institute of Chemical Technology (KRICT) core project (KK-1402-C0) funded by the Ministry of Science, ICT and Future Planning. This work was also supported by the Dongguk University Research Fund of 2014.

Notes and references

[a] Advanced Materials Division, Korea Research Institute of Chemical Technology (KRICT), 141 Gajeongro, Yuseong-gu, Daejeon 305-600, Republic of Korea. E-mail: youngmin@krict.re.kr (Y. Choi), sjeong@krict.re.kr (S. Jeong)
[b] Department of Physics, Dankook University, Cheonan 330-714, Korea
[c] Department of Materials Science and Engineering, Korea University, Seoul, Republic of Korea
[d] Division of Physics and Semiconductor Science, Dongguk University, Seoul, 100-715, Korea. E-mail: kbchung@dongguk.edu (K.-B. Chung)

Electronic supplementary information (ESI) available: Experimental details; the variation of mobility depending on a gate voltage; transfer characteristics for ZTO TFTs with channel layers annealed at different temperatures; HRTEM images, AFM images, XRD results, and XPS spectra near valence band for R0-, R1-, and R2-ZTO layers. See DOI: 10.1039/b000000x/

1 K. Nomura, H. Ohta, K. Ueda, T. Kamiya, M. Hirano, H. Hosono, *Science* 2003, **300**, 1269.
2. J. Y. Kim, S. H. Kim, H. H. Lee, K. Lee, W. Ma, X. Gong, A. J. Heeger, *Adv. Mater.* 2006, **18**, 572.
3 S. Jeong, J.-Y. Lee, S. S. Lee, S. W Oh, H. H. Lee, Y.-H. Seo, B.-H. Ryu, Y. Choi, *J. Mater. Chem.* 2011, **21**, 17066.
4 S. Jeong, J.-Y. Lee, S. S. Lee, Y.-H. Seo, S. Y. Kim, J.-U. Park, B.-H. Ryu, W. Yang, J. Moon, Y. Choi, *J. Mater. Chem. C* 2013, **1**, 4236.
5 Y. H. Hwang, J. S. Seo, J. M. Yun, H. Park, S. Yang, S. H. K. Park, B. S. Bae, *NPG Asia Mater.* 2013, **5**, e45.
6 S. Jeong, M. W Jung, J.-Y. Lee, H. Kim, J. Lim, K.-S. An, Y. Choi, S. S. Lee, *J. Mater. Chem. C* 2013, **1**, 5632.
7 K. K. Banger, R. L. Peterson, K. Mori, Y. Yamashita, T. Leedham, H. Sirringhaus, *Chem. Mater.* 2014, **26**, 1195.
8 S. Jeong, J. Moon, *J. Mater. Chem.* 2012, **22**, 1243.
9 K. K. Banger, Y. Yamashita, K. Mori, R. L. Peterson, T. Leedham, J. Rickard, H. Sirringhaus, *Nat. Mater.* 2011, **10**, 45.
10 G. Adamopoulos, A. Bashir, S. Thomas, W. P. Gillin, S. Georgakopoulos, M. Shkunov, M. A. Baklar, N. Stingelin, R. C. Maher, L. F. Cohen, D. D. C. Bradley, T. D. Anthopoulos, *Adv. Mater.* 2010, **22**, 4764.
11 S. Y. Park, B. J. Kim, K. Kim, M. S. Kang, K. H. Lim, T. I. Lee, J. M. Myoung, H. K. Baik, J. H. Cho, Y. S. Kim, *Adv. Mater.* 2012, **24**, 834.
12 Y. H. Kim, J. S. Heo, T. H. Kim, S. Park, M. H. Yoon, J. Kim, M. S. Oh, G. R. Yi, Y. Y. Noh, S. K. Park, *Nature* 2012, **489**, 128.
13 M.-G. Kim, M. G. Kanatzidis, A. Facchetti, T. J. Marks, *Nat. Mater.* 2011, **10**, 382.
14 M.-G. Kim, J. W. Hennek, H. S. Kim, M. G. Kanatzidis, A. Facchetti, T. J. Marks, *J. Am. Chem. Soc.* 2012, **134**, 11583.
15 J. W. Hennek, M.-G. Kim, M. G. Kanatzidis, A. Facchetti, T. J. Marks, *J. Am. Chem. Soc.* 2012, **134**, 9593.
16 J. W. Hennek, J. Smith, A. Yan, M.-G. Kim, W. Zhao, V. P. Dravid, A. Facchetti, T. J. Marks, *J. Am. Chem. Soc.* 2012, **135**, 10729.
17 Y. H. Kang, S. Jeong, J. M. Ko, J.-Y. Lee, Y. Choi, C. Lee, S. Y. Cho, *J. Mater. Chem. C* 2014, **2**, 4247.
18 S. T. Meyers, J. T. Anderson, C. M. Hung, J. Thompson, J. F. Wager, D. A. Keszler, *J. Am. Chem. Soc.* 2008, **130**, 17603.
19 S.-J. Seo, C. G. Choi, Y. H. Hwang, B.-S. Bae, *J. Phys. D: Appl. Phys.* 2009, **42**, 035106.

20 Y. J. Kim, B. S. Yang, S. Oh, S. J. Han, H. W. Lee, J. Heo, J. K. Jeong, H. J. Kim, *ACS Appl. Mater. Interfaces* 2013, **5**, 3255.
21 J.-S. Park, H. Kim, I.-D. Kim, *J.Electroceram.* 2014, **32**, 117.
22 S. Jeong, Y. G. Ha, J. Moon, A. Facchetti, T. J. Marks, *Adv. Mater.* 2010, **22**, 1346.
23 S. Jeong, J.-Y. Lee, S. S. Lee, Y. Choi, B.-H. Ryu, *J. Phys. Chem. C* 2011, **115**, 11773.
24 J. C. C. Fan, J. B. Goodenough, *J. Appl. Phys.* 1997, **48**, 3524.
25 T. Ishida, H. Kobayashi, Y. Nakato, *J. Appl. Phys.* 1993, **73**, 4344.
26 S. Yoon, Y. J. Tak, D. H. Yoon, U. H. Choi, J.-S. Park, B. D. Ahn, H. J. Kim, *ACS Appl. Mater. Interfaces* 2014, **6**, 13496.
27 Y. J. Tak, D. H. Yoon, S. Yoon, U. H. Choi, M. M. Sabri, B. D. Ahn, H. J. Kim, *ACS Appl. Mater. Interfaces* 2014, **6**, 6399.
28 W. H. Jeong, D. L. Kim, H. J. Kim, *ACS Appl. Mater. Interfaces* 2013, **5**, 9051.
29 S. Jeong, D. Kim, S. Lee, B.-K. Park, J. Moon, *Appl. Phys. Lett.* 2006, **89**, 092101.
30 K.-B. Chung, H. Seo, J. P. Long, G. Lucovsky, *Appl. Phys. Lett.* 2008, **93**, 182903.
31 H. Y. Jung, Y. Kang, A. Y. Hwang, C. K. Lee, S. Han, D. H. Kim, J. U. Bae, W. S. Shin, J. K. Jeong, *Sci. Rep.* 2014, **4**, 3765.
32 Y. S. Rim, B. D. Ahn, J.-S. Park, H.-J. Kim, *J. Phys. D* 2014, **47**, 045502.
33 B. K. Kim, J. S. Park, D. H. Kim, K.-B. Chung, *Appl. Phys. Lett.* 2014, **104**, 182106.
34 K.-B. Chung, J. P. Long, H. Seo, G. Lucovsky, D. Nordlund, *J. Appl. Phys.* 2009, **106**, 074102.
35 H. W. Park, J. S. Park, J. H. Lee, K. B. Chung, *Electrochem. Solid-State Lett.* 2012, **15**, H133.
36 G. Lucovsky, C. C. Fulton, Y. Zhang, Y. Zou, J. Luning, L. F. Edge, J. L. Whitten, R. J. Nemanich, H. Ade, D. G. Schlom, V. V. Afanase'v, A. Stesmans, S. Zollner, D. Triyoso, B.R. Rogers, *IEEE Trans. Device Mat.* 2005, **5**, 65.
37 K. Nomura, H. Ohta, A. Takagi, T. Kamiya, M. Hirano, H. Hosono, *Nature* 2004, **432**, 488.
38 T. Kamiya, K. Nomura, H. Hosono, *J. Disp. Technol.* 2009, **5**, 273.